ORIGINAL PAPER

Influence of Al_2O_3 particle size on properties of thermoplastic starch–TiO_2–Al_2O_3 composites

**Narong Chueangchayaphan[1] · Kang Ai Ting[2] · Mahani Yusoff[2] ·
Wannarat Chueangchayaphan[1]**

© Springer-Verlag GmbH Germany, part of Springer Nature 2019

Abstract

Thermoplastic starch (TPS), an inexpensive, renewable, widely available and biodegradable biopolymer, has been promoted as a promising alternative to synthetic polymers based on fossil resources. However, it exhibits weak mechanical properties and high moisture uptake. Reinforcing fillers have been used to improve the properties of thermoplastic starch. This work studies the effects of Al_2O_3 particle size on dielectric, thermal, physical, mechanical and morphological properties of thermoplastic starch–TiO_2–Al_2O_3 composites at the fixed TPS:TiO_2:Al_2O_3 weight ratio 97:2:1. The Al_2O_3 particle sizes tested were 0.05 μm, 1 μm and 5 μm. Dielectric, thermal, mechanical and morphological properties were determined. With increasing Al_2O_3 particle size, slight increases were observed in contact angle, hardness and thermal stability, while dielectric constant, dissipation factor and glass transition temperature decreased. However, the Al_2O_3 particle size did not significantly affect tensile properties. Scanning electron microscopy was used to investigate the morphology in the composites. In summary, the incorporation of TiO_2 and Al_2O_3 in thermoplastic starch could extend its potential in flexible films, compost bags and packaging applications.

Keywords Thermoplastic starch · Particle size · Titanium dioxide · Aluminum oxide · Cassava starch

✉ Wannarat Chueangchayaphan
   wannarat.p@psu.ac.th

1 Faculty of Science and Industrial Technology, Prince of Songkla University, Surat Thani Campus, Surat Thani 84000, Thailand

2 Faculty of Bioengineering and Technology, Universiti Malaysia Kelantan, Jeli Campus, 17600 Jeli, Kelantan, Malaysia

Introduction

Starch is employed in numerous industrial applications on making food and non-food products, owing to its low cost, availability and ability to impart a broad range of functional properties. Starch has become a most promising candidate for future materials and alternatives to the fossil resources that have recycling limitations and cause environmental concerns, because of its attractive cost and performance [1, 2]. Starch is composed of both amylose molecules and amylopectin molecules with α-(1–4)-linked D-glucose backbones and α-(1–6)-linked branches. Native starch from plants is granular and partly crystalline and is not suitable for thermoplastic materials. When a plasticizer (typically water) is added, gelatinization will occur under heat and high shear, and the native granular starch is disrupted and converted to thermoplastic starch (TPS) that can be processed similarly to other more conventional thermoplastic polymers [3–7]. Various sources of starch have been extensively investigated to obtain biodegradable thermoplastic starch, such as potato starch [3, 8], corn starch [8], rice starch [9] and wheat starch [10]. Cassava or tapioca is among the most important starch sources in the tropics and is extensively used in tropical Africa and South America as well as parts of Asia, especially Indonesia and Thailand [11]. Thailand was one of the top five producers globally in 2012 [12]. In addition, cassava flour is substantially rich in starch with only small amounts of other components and is a good source of inexpensive good purity starch [13]. Thermoplastic cassava starch has been prepared for bioactive, biodegradable, flexible and edible films or packages [8, 14–19].

However, TPS has as its disadvantages: brittleness, poor mechanical properties, high water sensitivity and poor barrier properties [20]. To improve the properties of thermoplastic starch, it is blended with other polymers, such as natural rubber [21], polystyrene [22], polyvinyl alcohol [23–25], polyethylene [26], polypropylene [27], polylactic acid [28–30], polycaprolactone [31], chitosan [32, 33], poly(butylene adipate-co-terephthalate) [34], or polyhydroxyalkanoates [35], and reinforced with organic or mineral fillers, such as cellulose [3, 36–41], talc [42], or clay [43, 44], ZnO [45]. Titanium dioxide (TiO_2) is a multipurpose filler used with polymer matrices, and is nontoxic, inert and inexpensive with inherent photocatalytic activity against microorganisms, staining, allergens and odors [46]. Several studies have assessed the influences of TiO_2 addition on the properties of various biopolymers. For example, Zhu et al. [47] prepared poly(lactic acid)/TiO_2 composite films. It was found that the addition of TiO_2 nanoparticles increased tensile strength and crystallinity, as well as improved the barrier properties. Amin and Panhuis [48] found that the mechanical properties and water resistance were improved by addition of TiO_2 in chitosan matrix. Khan et al. [49] prepared regenerated bacterial cellulose/TiO_2 nanocomposites to enhance bactericidal activity and tissue regeneration properties. Oleyaei et al. [46] studied the effects of TiO_2 concentration on functional, UV transmittance and mechanical properties of potato starch/TiO_2 nanocomposite films, with a view to food packaging applications. Ostafińska et al. (2017) prepared thermoplastic starch/TiO_2 composites

with highly homogenous good dispersion of the filler by a two-step method, including solution casting followed by melt mixing. The modulus increased with TiO_2 loading [50]. Aluminum oxide (Al_2O_3) or alumina is commonly used as filler in commercial applications due to its low cost, electrical insulation ability, and high temperature tolerance [51]. The incorporation of Al_2O_3 has been reported for polymer matrices including natural rubber [52], silicon rubber [53], poly(lactic acid) [54], epoxy [55], and chitosan [56, 57].

Individually TiO_2 or Al_2O_3 fillers improve the properties of polymers. Combinations of TiO_2 and Al_2O_3 have been used to enhance the properties of thermoplastic starch composites. The aim of this work was to study the effects of Al_2O_3 filler particle size on dielectric, mechanical, morphology and thermal properties of thermoplastic starch–TiO_2–Al_2O_3 composites.

Experimental

Materials

Food grade native cassava starch was provided by Kriangkrai Co., Ltd., Thailand. It was first heated for 24 h in a vacuum oven at 60–70 °C to remove moisture and was immediately placed in a desiccator to prevent moisture re-absorption. The glycerol used as a plasticizer had 1.26 g/cm^3 density and was manufactured by Unilever Co., Ltd., USA. Titanium dioxide (TiO_2) nanopowder (< 100 nm, mixture of rutile and anatase TiO_2) and alumina, Al_2O_3 (0.05 μm, 1 μm and 5 μm) were purchased from Sigma-Aldrich Co.

Preparation of TPS composites

Native cassava starch was weighed and introduced in a kitchen blender. Glycerol was then added and continuously pre-mixed at room temperature and 1000 rpm for 10 min to obtain a homogeneous dispersion. The weight ratio of glycerol and cassava starch was 30:70. The mixture was placed in a desiccator for 24 h, after which it was further dry-mixed with TiO_2 and Al_2O_3 particles. The weight ratio TPS:TiO_2:Al_2O_3 was held fixed at 97:2:1. In order to obtain thermoplastic starch (TPS), the mixture was continuously melt blended in an internal mixer at 140 °C with 60 rpm rotor speed for 6 min. During mixing, the torque was monitored, in order to assess plasticization and processability of the starch. The starch lost its original granular structure and was transformed into a molten homogeneous TPS. The TPS composite was sheeted out on a two-roll mill, and 1-mm-thick sheets were prepared by 1500 psi compression at 165 °C for 15 min.

Testing mechanical properties

Tensile testing was performed to characterize the mechanical properties of the thermoplastic starch composites, using a Hounsfield Tensometer, model H 10 KS. The

sample sheet was cut by a cutting machine into the dumbbell shape specified in ASTM D680-14 standard [58]. Specimens were tested for each formula at 25 °C with a cross-head speed of 500 mm/min. The stress–strain curves are reported. The tensile strength (σ_b) and elongation at break (ε_b) were determined from the curves. The Young's modulus (E) was determined as the initial slope of the linear portion of each stress–strain curve. The Shore A hardness was measured according to ASTM D2240-15 with an indentation durometer [59].

Sample characterization

Thermogravimetric analysis was performed on a TA Instruments® TGA Q 500 with a heating rate of 10 °C/min from room temperature to 600 °C in nitrogen atmosphere. Dynamic mechanical thermal analysis used a Rheometric Scientific® DMTA V. The experiment was carried out in the dual-cantilever bending mode at a frequency of 1 Hz with 0.01% strain amplitude, and the heating rate was 3 °C/min. The temperature range was from − 120 to 80 °C. Dielectric constant (ε') and dissipation factor or dielectric loss tangent (tan δ) were obtained by dielectric measurements. The sample with ~ 1 mm thickness was coated with high-purity silver paint before measurement with Precision LCR meter (Agilent, model 4285A) at room temperature in the frequency range from 75 kHz to 30 MHz. The evaluation of the dispersion of fillers in TPS was performed by using a scanning electron microscope (SEM) (FEI Quanta, 400, USA). Fresh cross sections were obtained by fracturing after immersion in liquid nitrogen. All specimens were sputter coated with gold prior to SEM examination.

Results and discussion

Dielectric constant and dissipation factor

The dielectric constant and dissipation factor over the frequency range from 75 kHz to 30 MHz are shown in Fig. 1, for the thermoplastic starch–TiO_2–Al_2O_3 composites with Al_2O_3 particle sizes 0.05 μm, 1 μm, and 5 μm. The dielectric constant rapidly decreased at low frequency and then gradually decreased at frequencies above 2 MHz. This behavior was almost similar in all cases tested. At low frequencies, maximal polarization was possible [60], while the dissipation factor rapidly decreased with frequency in the low range (0–10 MHz), because both ionic relaxation and dipole relaxation are comparatively slow. The further increase in dissipation factor at the higher frequencies (> 10 MHz) might be due to relaxation of polar groups and ionic polymerization. The polar molecules cannot orient rapidly enough as the electromagnetic frequency is increased [61]. The dielectric constant decreased with Al_2O_3 particle size. The larger particles had lower specific surface and therefore less interfacial polarization. Thus, the smaller Al_2O_3 particles had comparatively improved dielectric properties in the thermoplastic starch–TiO_2–Al_2O_3 composites, with also stronger mechanical stress effects and extrinsic grain boundary
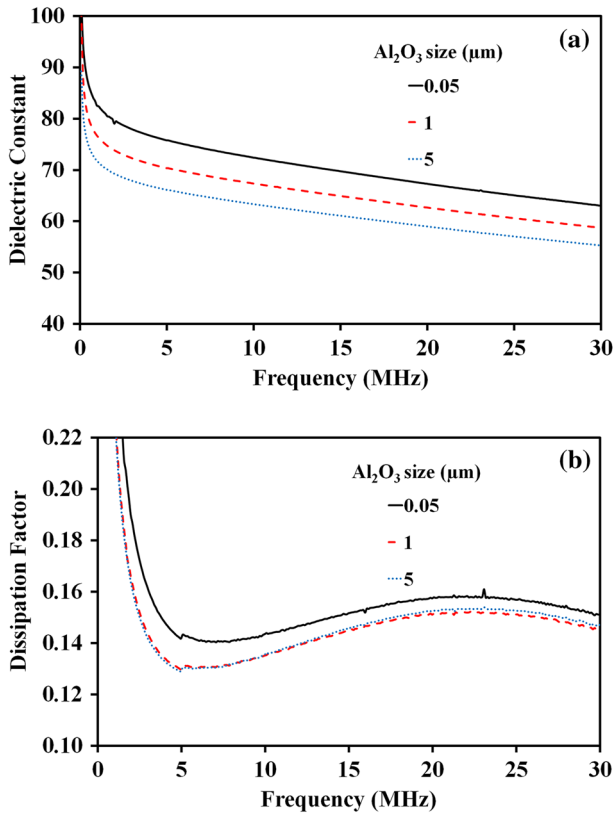
Fig. 1 The frequency dependence of **a** dielectric constant and **b** dissipation factor for the thermoplastic starch–TiO$_2$–Al$_2$O$_3$ composites with different Al$_2$O$_3$ particle sizes

effects [62]. In addition, the polarization contribution by dipole–dipole interactions increased with closely packed particles, and the smaller particles had better particle–particle contacts and increased packing density [63].

Thermal analysis

Figure 2 exhibits the TGA and DTA of thermoplastic starch–TiO$_2$–Al$_2$O$_3$ composites, respectively. All the samples showed two main stages in the loss of mass. Within the temperature range from 30 to 280 °C, the loss corresponded to the volatilization of both water and glycerol from the TPS. The second stage corresponded to starch decomposition (280–350 °C) [64]. Finally, the char yield at 600 °C was similar for all the samples because they had the same mixture proportions. As can be observed in Fig. 2a, TGA curves showed that increased Al$_2$O$_3$ particle size improved thermal stability of the composites. The DTA curves (Fig. 2b) show the thermal degradation characteristics more clearly. The maximum decomposition peaks in the DTA curves slightly shifted toward higher temperature as the particle size of Al$_2$O$_3$
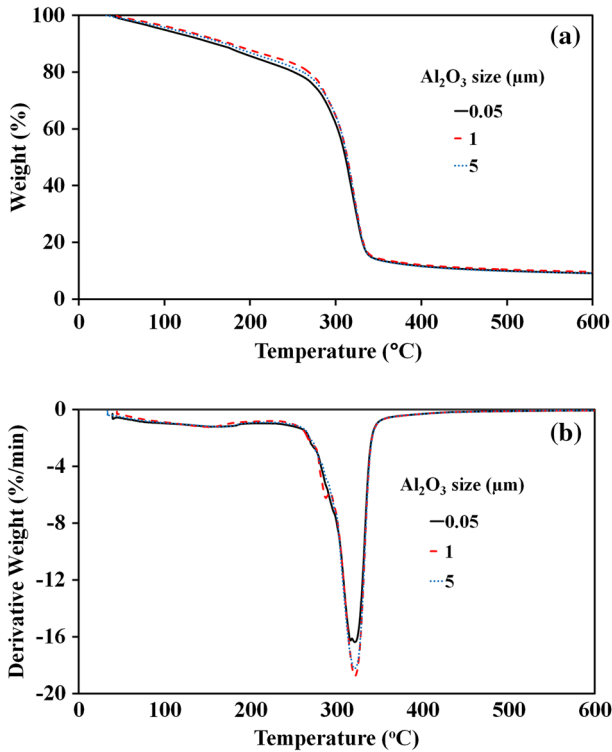
Fig. 2 **a** TGA and **b** DTA of thermoplastic starch–TiO$_2$–Al$_2$O$_3$ composites with different Al$_2$O$_3$ particle sizes

increased, which agrees with the results from TGA. The maximum decomposition (DTA$_{max}$) peak with larger Al$_2$O$_3$ particles was lower than with smaller particles, indicating that the larger Al$_2$O$_3$ particles increased the rate of degradation of starch.

Dynamic mechanical thermal analysis

Storage modulus (E') and loss modulus (E'') are related to stiffness, representing elastic and viscous components in deformation response, respectively, while the loss factor (tan δ) relates to molecular motions [65]; these are shown in Fig. 3. Figure 3a shows the storage modulus (E') as a function of temperature for the thermoplastic starch–TiO$_2$–Al$_2$O$_3$ composites with different Al$_2$O$_3$ particle sizes. Thermoplastic starch filled with 5 μm Al$_2$O$_3$ provided higher storage modulus than the other cases. Glass transition temperature (T_g) was determined from the maximum peak of tan δ and is presented in Table 1 and Fig. 3c. Two T_g values were detected. The first one is attributed to relaxation of glycerol rich phases and did not significantly change with Al$_2$O$_3$ particle size. The second relaxation is attributed to starch chain mobility and exhibited clear changes, indicating that Al$_2$O$_3$ can interact with starch rich phases more strongly than with glycerol rich phases [66]. It was found that the
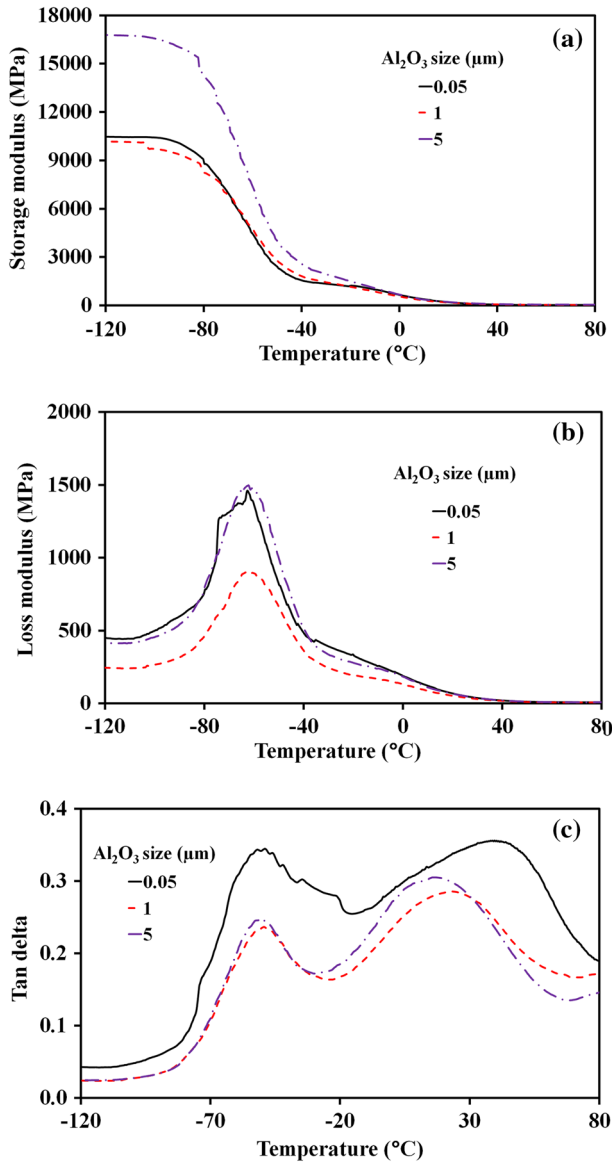
Fig. 3 Evolution of **a** storage modulus, **b** loss modulus and **c** tan δ with temperature for thermoplastic starch–TiO$_2$–Al$_2$O$_3$ composites with different Al$_2$O$_3$ particle sizes

second relaxation of starch rich phases shifted to lower temperatures with increasing Al$_2$O$_3$ particle size, indicating that small-sized Al$_2$O$_3$ filler hindered chain mobility of starch. This suggests that good dispersion of the finer filler was achieved. T_g tended to decrease with Al$_2$O$_3$ particle size, from 39.6 °C with 0.05 μm Al$_2$O$_3$ to 15.1 °C with 5 μm Al$_2$O$_3$ as seen in Table 1. The increased T_g with smaller Al$_2$O$_3$

Table 1 Tensile properties and glass transition temperature of the thermoplastic starch–TiO$_2$–Al$_2$O$_3$ composites with different Al$_2$O$_3$ particle sizes

| Al$_2$O$_3$ size (µm)	Tensile properties			T_g from DMTA	
	E (MPa)	σ_b (MPa)	ε_b (%)	T_{g1} (°C)	T_{g2} (°C)
0.05	4.2 ± 1.7	1.7 ± 0.3	129.8 ± 20.8	− 52.0	39.6
1	5.9 ± 1.9	1.5 ± 0.1	166.2 ± 16.6	− 49.0	22.8
5	5.8 ± 2.1	1.2 ± 0.2	173.0 ± 38.2	− 50.7	15.1

particles was attributed to increased interfacial interactions with the polymer matrix, because the finer particles had higher specific surface and restricted molecular chain motions by the interactions [67]. However, the T_g of these thermoplastic starch composites was not detectable by DSC. Zhang et al. [68] reported that DSC is not sensitive enough to measure the heat-flow changes of starch samples.

Contact angle

The hydrophilicity of material surfaces can be characterized by water droplet contact angles. A low contact angle indicates high hydrophilicity. The contact angles for the thermoplastic starches with different sized Al$_2$O$_3$ fillers are shown in Fig. 4. It was found that the contact angle increased with Al$_2$O$_3$ particle size, indicating that the composite surface became more hydrophobic.

Scanning electron microscopy

Figure 5 exhibits SEM images of native cassava starch and fracture surfaces for the thermoplastic starch matrix and the thermoplastic starch–TiO$_2$–Al$_2$O$_3$ composites, at 2500× magnification. Spherical and truncated shapes and some oval shapes were
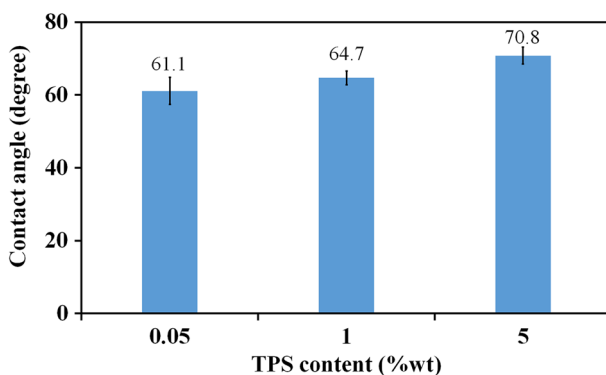
Fig. 4 Water contact angles on the thermoplastic starch–TiO$_2$–Al$_2$O$_3$ composites with different Al$_2$O$_3$ particle sizes
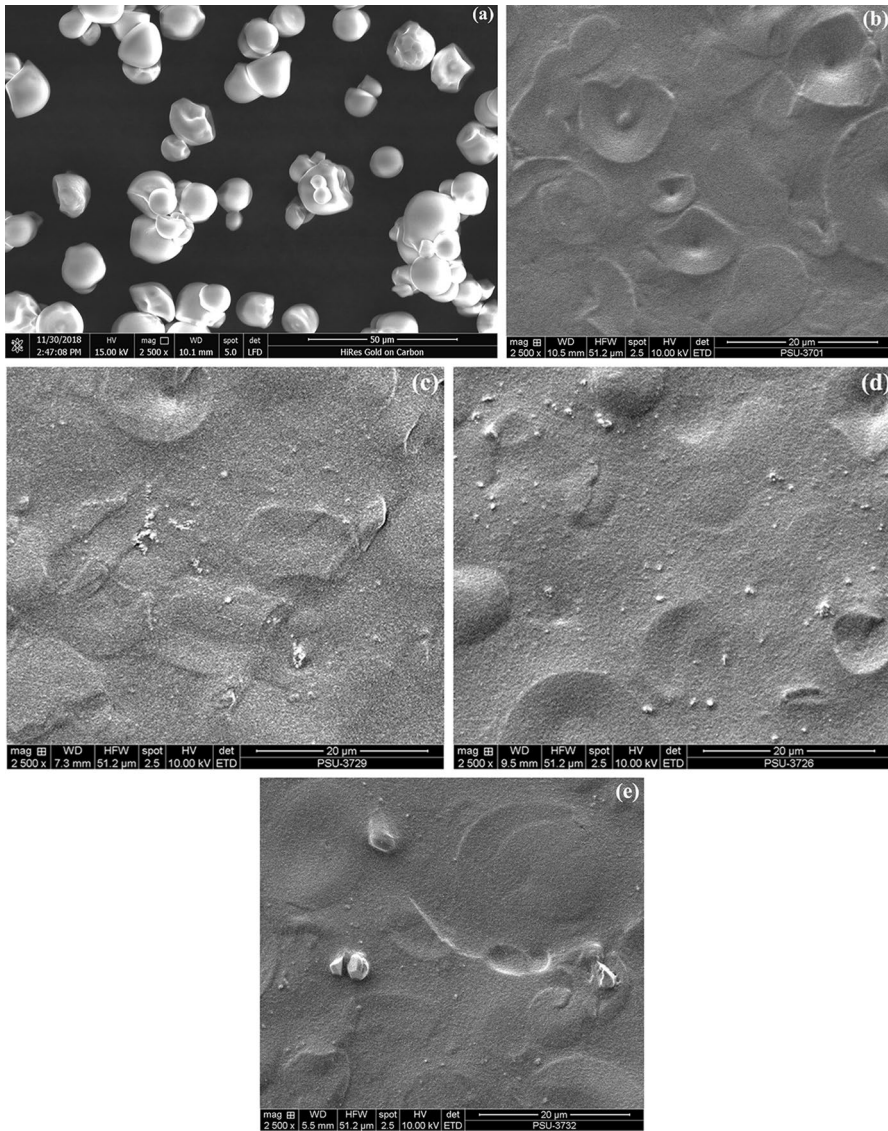
Fig. 5 SEM images of **a** native cassava starch, **b** pure TPS, and of the TPS–TiO$_2$–Al$_2$O$_3$ composites with Al$_2$O$_3$ particle sizes, **c** 0.05 μm, **d** 1 μm and **e** 5 μm

observed for the native cassava starch granules shown in Fig. 5a. In addition, various size granules and agglomerates were found, as results reported also earlier [69, 70]. After adding glycerol and under heat and high shear, the original granular structure was transformed into a molten homogeneous TPS, as seen in Fig. 5b. The fracture surface of thermoplastic starch had holes and remnants of starch granules. However, no cracks were observed in any of the samples. Furthermore, good adhesion between

the fillers and TPS phase is likely, since no holes or voids are seen from loss of filler particles. The smaller Al_2O_3 particles were more homogeneously dispersed in the TPS phase than the larger particles that tended to agglomerate, as seen in Fig. 5e.

Mechanical properties

Nonlinear stress–strain curves are seen in Fig. 6. The stress continuously increased with strain until breakage without necking, indicating typical plastic behavior [71]. Young's modulus, tensile strength and elongation at break are summarized in Table 1.

The modulus refers to the stiffness of the material. It is obtained from the ratio of stress and strain in elastic region of the stress–strain curve. It was found that the particle size of Al_2O_3 in the range studied did not affect the Young's modulus. Similar lack of particle size effects on the elastic modulus has been reported for epoxy resin–alumina trihydrate composite (1, 2, 5, 8 and 12 μm) [72] and for polyester-aluminum composite (100 nm, 3.5 and 20 μm) [73]. When the particle size is larger than a critical limit, it will not affect modulus of the composite. In addition, the tensile strength tended to decrease with filler particle size because the larger particles had lower specific surface and less efficient stress transfer [74]. Furthermore, the larger Al_2O_3 particles improved the matrix surface resistance to indentation, as the surface hardness of a composite mainly is attributed to hardness of the solid filler [75]. Thus, hardness increased with Al_2O_3 particle size because of increased contact of the filler, as seen in Fig. 7.

Conclusions

Biocomposites based on thermoplastic cassava starch containing TiO_2 and Al_2O_3 combination filler, with varied Al_2O_3 particle size (0.05 μm, 1 μm or 5 μm), were successfully prepared by melt mixing in an internal mixer followed by
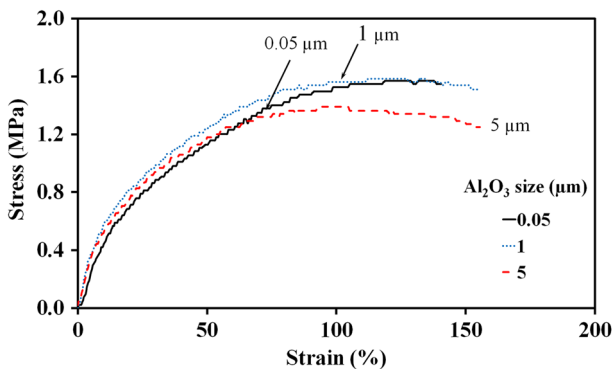
Fig. 6 Stress-strain curves of the thermoplastic starch–TiO_2–Al_2O_3 composites with different Al_2O_3 particle sizes
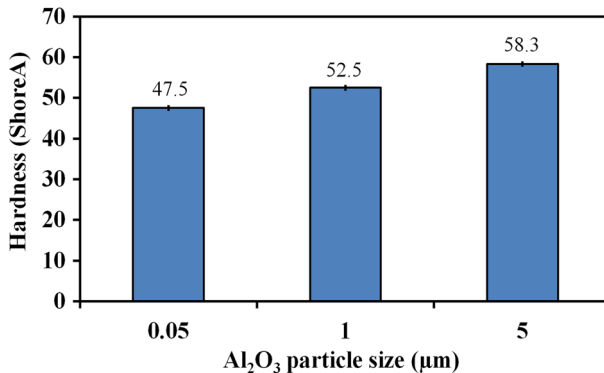
Fig. 7 Hardness of the thermoplastic starch–TiO₂–Al₂O₃ composites with different Al₂O₃ particle sizes

thermo-compression. The results showed that water contact angle, hardness and thermal stability slightly increased, whereas dielectric constant, dissipation factor and glass transition temperature decreased with Al₂O₃ particle size. However, the tensile properties were not significantly affected by Al₂O₃ particle size. Aggregates of the larger sized Al₂O₃ particles were observed in SEM images.

References

1. Bertolini AC (2010) Starches: characterization, properties, and applications. CRC Press, Florida, p 6
2. Zhang S, Lin Z, Jiang G, Wang J, Wang DY (2018) Construction of chelation structure between Ca²⁺ and starch via reactive extrusion for improving the performances of thermoplastic starch. Compos Sci Technol 159:59–69
3. Balakrishnan P, Sreekala MS, Kunaver M, Huskić M, Thomas S (2017) Morphology, transport characteristics and viscoelastic polymer chain confinement in nanocomposites based on thermoplastic potato starch and cellulose nanofibers from pineapple leaf. Carbohydr Polym 169:176–188
4. Jumaidin R, Sapuan SM, Jawaid M, Ishak MR, Sahari J (2017) Effect of seaweed on mechanical, thermal, and biodegradation properties of thermoplastic sugar palm starch/agar composites. Int J Biol Macromol 99:265–273
5. Lendvai L, Apostolov A, Kocsis JK (2017) Characterization of layered silicate-reinforced blends of thermoplastic starch (TPS) and poly(butylene adipate-co-terephthalate). Carbohydr Polym 173:566–572
6. Pardo IM, Shanks RA, Adhikari B, Adhikari R (2017) Thermoplastic starch-nanohybrid films with polyhedral oligomeric silsesquioxane. Carbohydr Polym 173:170–177
7. Yang J, Tang K, Qin G, Chen Y, Peng L, Wan X, Xiao H, Xia Q (2017) Hydrogen bonding energy determined by molecular dynamics simulation and correlation to properties of thermoplastic starch films. Carbohydr Polym 166:256–263
8. Bergel BF, Luz LM, Santana RMC (2017) Comparative study of the influence of chitosan as coating of thermoplastic starch foam from potato, cassava and corn starch. Prog Org Coat 106:27–32
9. Prachayawarakorn J, Sangnitidej P, Boonpasith P (2010) Properties of thermoplastic rice starch composites reinforced by cotton fiber or low-density polyethylene. Carbohydr Polym 81:425–433

10. Kelnar I, Kaprálková L, Brožová L, Hromádková J, Kotek J (2013) Effect of chitosan on the behaviour of the wheat B-starch nanocomposite. Ind Crops Prod 46:186–190

11. Charoenkul N, Uttapap D, Pathipanawat W, Takeda Y (2011) Physicochemical characteristics of starches and flours from cassava varieties having different cooked root textures. LWT Food Sci Technol 44:1774–1781

12. Zhu F (2015) Composition, structure, physicochemical properties, and modifications of cassava starch. Carbohydr Polym 122:456–480

13. Tanetrungroj Y, Prachayawarakorn J (2015) Effect of starch types on properties of biodegradable polymer based on thermoplastic starch process by injection molding technique. Songklanakarin J Sci Technol 32(2):193–199

14. Teixeira EM, Róz AL, Carvalho AJF, Curvelo AAS (2007) The effect of glycerol/sugar/water and sugar/water mixtures on the plasticization of thermoplastic cassava starch. Carbohydr Polym 69:619–624

15. Prachayawarakorn J, Pomdage W (2014) Effect of carrageenan on properties of biodegradable thermoplastic cassava starch/low-density polyethylene composites reinforced by cotton fibers. Mater Des 61:264–269

16. Jaramillo CM, Gutiérrez TJ, Goyanes S, Bernal C, Famá L (2016) Biodegradability and plasticizing effect of yerba mate extract on cassava starch edible films. Carbohydr Polym 151:150–159

17. Monteiro MKS, Oliveira VRL, Santos FKG, Neto ELB, Leite RHL, Aroucha EMM, Silva RR, Silva KNO (2018) Incorporation of bentonite clay in cassava starch films for the reduction of water vapor permeability. Food Res Int 105:637–644

18. Clasen SH, Müller CMO, Parize AL, Pires ATN (2018) Synthesis and characterization of cassava starch with maleic acid derivatives by etherification reaction. Carbohydr Polym 180:348–353

19. Campos A, Neto ARS, Rodrigues VB, Luchesi BR, Mattoso LHC, Marconcini JM (2018) Effect of raw and chemically treated oil palm mesocarp fibers on thermoplastic cassava starch properties. Ind Crops Prod 124:149–154

20. Nasrabadi BN, Behzad T, Bagheri R (2014) Preparation and characterization of cellulose nanofiber reinforced thermoplastic starch composites. Fiber Polym 15(2):347–354

21. Carvalho AJF, Job AE, Alves N, Curvelo AAS, Gandini A (2003) Thermoplastic starch/natural rubber blends. Carbohydr Polym 53:95–99

22. Schlemmer D, Sales MJA, Resck IS (2009) Degradation of different polystyrene/thermoplastic starch blends buried in soil. Carbohydr Polym 75:58–62

23. Ardakani KM, Nazari B (2010) Improving the mechanical properties of thermoplastic starch/poly(vinyl alcohol)/clay nanocomposites. Compos Sci Technol 70:1557–1563

24. Liu Z, Dong Y, Men H, Jiang M, Tong J, Zhou J (2012) Post-crosslinking modification of thermoplastic starch/PVA blend films by using sodium hexametaphosphate. Carbohydr Polym 89:473–477

25. Tian H, Yan J, Rajulu AV, Xiang A, Luo X (2017) Fabrication and properties of polyvinyl alcohol/starch blend films: effect of composition and humidity. Int J Biol Macromol 96:518–523

26. Cerclé C, Sarazin P, Favis BD (2013) High performance polyethylene/thermoplastic starch blends through controlled emulsification phenomena. Carbohydr Polym 92:138–148

27. Ferreira WH, Khalili RR, Figueira Junior MJM, Andrade CT (2014) Effect of organoclay on blends of individually plasticized thermoplastic starch and polypropylene. Ind Crops Prod 52:38–45

28. Yang Y, Tang Z, Xiong Z, Zhe J (2015) Preparation and characterization of thermoplastic starches and their blends with poly(lactic acid). Int J Biol Macromol 77:273–279

29. Akrami M, Ghasemi I, Azizi H, Karrabi M, Seyedabadi M (2016) A new approach in compatibilization of the poly(lactic acid)/thermoplastic starch (PLA/TPS) blends. Carbohydr Polym 144:254–262

30. Lv S, Zhang Y, Gu J, Tan H (2018) Soil burial-induced chemical and thermal changes in starch/poly(lactic acid) composites. Int J Biol Macromol 113:338–344

31. Mahieu A, Terrié C, Youssef B (2015) Thermoplastic starch films and thermoplastic starch/polycaprolactone blends with oxygen-scavenging properties: influence of water content. Ind Crops Prod 72:192–199

32. Mendes JF, Paschoalin RT, Carmona VB, Neto ARS, Marques ACP, Marconcini JM, Mattoso LHC, Medeiros ES, Oliveira JE (2016) Biodegradable polymer blends based on corn starch and thermoplastic chitosan processed by extrusion. Carbohydr Polym 137:452–458

33. Ren L, Yan X, Zhou J, Tong J, Su X (2017) Influence of chitosan concentration on mechanical and barrier properties of corn starch/chitosan films. Int J Biol Macromol 105:1636–1643

34. Marinho VAD, Pereira CAB, Vitorino MBC, Silva AS, Carvalho LH, Candedo EL (2017) Degradation and recovery in poly(butylene adipate-co-terephthalate)/thermoplastic starch blends. Polym Test 58:166–172

35. Xu P, Zeng Q, Cao Y, Ma P, Dong W, Chen M (2017) Interfacial modification on polyhydroxyalkanoates/starch blend by grafting in-situ. Carbohydr Polym 174:716–722

36. Martins IMG, Magina SP, Oliveira L, Freire CSR, Silvestre AJD, Neto CP, Gandini A (2013) New biocomposites based on thermoplastic starch and bacterial cellulose. Compos Sci Technol 69:2163–2168

37. Hietala M, Mathew AP, Oksman K (2013) Bionanocomposites of thermoplastic starch and cellulose nanofibers manufactured using twin-screw extrusion. Eur Polym J 49:950–956

38. González K, Retegi A, González A, Eceiza A, Gabilondo N (2015) Starch and cellulose nanocrystals together into thermoplastic starch bionanocomposites. Carbohydr Polym 117:83–90

39. Karimi S, Abdulkhani A, Tahir PM, Dufresne A (2016) Effect of cellulosic fiber scale on linear and non-linear mechanical performance of starch-based composites. Int J Biol Macromol 91:1040–1044

40. Ghanbari A, Tabarsa T, Ashori A, Shakeri A, Mashkour M (2018) Preparation and characterization of thermoplastic starch and cellulose nanofibers as green nanocomposites: extrusion processing. Int J Biol Macromol 112:442–447

41. Fazeli M, Keley M, Biazar E (2018) Preparation and characterization of starch-based composite films reinforced by cellulose nanofibers. Int J Biol Macromol 116:272–280

42. López OV, Castillo LA, García MA, Villar MA, Barbosa SE (2015) Food packaging bags based on thermoplastic corn starch reinforced with talc nanoparticles. Food Hydrocoll 43:18–24

43. Dean K, Yu L, Wu DY (2007) Preparation and characterization of melt-extruded thermoplastic starch/clay nanocomposites. Compos Sci Technol 67:413–421

44. Requena VHC, Rivas BL, Pérez MA, Figueroa CR, FigueroaN E, Sanfuentes EA (2017) Thermoplastic starch/clay nanocomposites loaded with essential oil constituents as packaging for strawberries—In vivo antimicrobial synergy over Botrytis cinerea. Postharvest Biol Technol 129:29–36

45. Guz L, Famá L, Candal R, Goyanes S (2017) Size effect of ZnO nanorods on physicochemical properties of plasticized starch composites. Carbohydr Polym 157:1611–1619

46. Oleyaei SA, Zahedi Y, Ghanbarzadeh B, Moayedi AA (2016) Modification of physicochemical and thermal properties of starch films by incorporation of TiO_2 nanoparticles. Int J Biol Macromol 89:256–264

47. Zhu Y, Buonocore GG, Lavorgna M, Ambrosio L (2011) Poly(lactic acid)/titanium dioxide nanocomposite films: influence of processing procedure on dispersion of titanium dioside and photocatalytic activity. Polym Compos 32(4):519–528

48. Amin KAM, Panhuis M (2012) Reinforced materials based on chitosan, TiO_2 and Ag composites. Polymers 4:590–599

49. Khan S, Ul-Islam M, Khattak WA, Ullah MW, Park JK (2015) Bacterial cellulose-titanium dioxide nanocomposites: nanostructural characteristics, antibacterial mechanism, and biocompatibility. Cellulose 22:565–579

50. Ostafińska A, Mikešová J, Krejčíková S, Nevoralová M, Šturcová A, Zhigunov A, Michálková D, Šlouf M (2017) Thermoplastic starch composites with TiO_2 particles: preparation, morphology, rheology and mechanical properties. Int J Biol Macromol 101:273–282

51. Chen JP, Liu T, Zhang J, Wang BB, Ying J, Liu F, Zhang XB (2014) Influence of phase and morphology on thermal conductivity of alumina particle/silicone rubber composites. Appl Phys A Mater Sci Process 117:1985–1992

52. Tangboriboon N, Uttanawanit N, Longtong M, Wongpinthong P, Sirivat A, Kunanuruksapong R (2010) Electrical and electrorheological properties of alumina/natural rubber (STR XL) composites. Materials 3:656–671

53. Venkatesulu B, Thomas MJ (2010) Erosion resistance of alumina-filled silicone rubber nanocomposites. IEEE Trans Dielectr Electr Insul 17(2):615–624

54. Kurtycz P, Ciach T, Olszyna A, Kunicki A, Roslon M, Wilczynska JD, Nowak K, Anuszewska E (2013) Electrospun poly(L-lactic) acid/nanoalumina (PLA/Al_2O_3) composite fiber mats with potential biomedical application- Investigation of cytotoxicity. Fiber Polym 14(4):578–583

55. Verma V, Shukla DK, Kumar V (2014) Estimation of fatique life of epoxy-alumina polymer nanocomposites. Proc Mater Sci 5:669–678

56. Gandhi MR, Viswanathan N, Meenakshi S (2010) Preparation and application of alumina/chitosan biocomposite. Int J Biol Macromol 47:146–154

57. Golie WM, Upadhyayula S (2017) An investigation on biosorption of nitrate from water by chitosan based organic-inorganic hybrid biocomposites. Int J Biol Macromol 97:489–502

58. ASTM (2014) Proceedings of the D638-14. Standard test method for tensile properties of plastics, ASTM International, West Conshohocken

59. ASTM (2015) Proceedings of the D2240-15. Standard test method for rubber property—durometer hardness. ASTM International, West Conshohocken

60. Kumar ER, Kamzin AS, Prakash T (2015) Effect of particle size on structural, magnetic and dielectric properties of manganese substituted nickel ferrite nanoparticles. J Magn Magn Mater 378:389–396

61. Motwani T, Seetharaman K, Anantheswaran RC (2007) Dielectric properties of starch slurries as influenced by starch concentration and gelatinization. Carbohydr Polym 67:73–79

62. Chi QG, Dong JF, Liu GY, Chen Y, Wang X, Lei QQ (2015) Effect of particle size on the dielectric properties of $0.5Ba(Zr_{0.2}Ti_{0.8})O_3$–0.5 $(Ba_{0.7}Ca_{0.8})TiO_3$/polyvinylidene fluoride hybrid films. Ceram Int 41(10):15116–15121

63. Yoon JR, Han JW, Lee KM, Lee HY (2009) Dielectric properties of polymer-ceramic capacitors. Trans Electr Electron Mater 10(4):116–120

64. Xiaofei M, Jiugao Y, Jin F (2004) Urea and formamide as a mixed plasticizer for thermoplastic starch. Polym Int 53:1780–1785

65. Lopez O, Garcia MA, Villar MA, Gentili A, Rodriguez MS, Albertengo L (2014) Thermo-compression of biodegradable thermoplastic corn starch films containing chitin and chitosan. LWT Food Sci Technol 57:106–115

66. Salaberria AM, Labidi J, Fernandes SCM (2014) Chitin nanocrystals and nanofibers as nano-sized fillers into thermoplastic starch-based biocomposites processed by melt-mixing. Chem Eng J 256:356–364

67. Liawthanyarat N, Rimdusit S (2015) Effects of particles size of nanosilica on properties of polybenzoxazine nanocomposites. Key Eng Mater 659:394–398

68. Zhang Y, Rempel C, Liu Q (2014) Thermoplastic starch processing and characteristics-A review. Crit Rev Food Sci Nutr 54(10):1353–1370

69. Horstmann SW, Belz MCE, Heitmann M, Zannini E, Arendt EK (2016) Fundamental study on the impact of gluten-free starches on the quality of gluten-free model breads. Foods 5(1–12):30

70. Mendoza JS, Urzola SP, Rhenals DL, Flórez JF (2018) Enzymatic modification of cassava starch (Corpoica M-Tai) around the pasting temperature. DYNA 85(204):223–230

71. Schmitt H, Guidez A, Prashantha K, Soulestin J, Lacrampe MF, Krawczak P (2015) Studies on the effect of storage time and plasticizers on the structural variations in thermoplastic starch. Carbohydr Polym 115:364–372

72. Radford KC (1971) The mechanical properties of an epoxy resin with a second phase dispersion. J Mater Sci 6:1286–1291

73. Singh RP, Zhang M, Chan D (2002) Toughening of a brittle thermosetting polymer: effects of reinforcement particle size and volume fraction. J Mater Sci 37:781–788

74. Fu SY, Feng XQ, Lauke B, Mai YW (2008) Effects of particle size, particle/matrix interface adhesion and particle loading on mechanical properties of particulate–polymer composites. Compos Part B Eng 39(6):933–961

75. Mohamed MA, Shaltout NA, El Miligy AA (2011) The effect of gamma irradiation and particle size of $CaCO_3$ on the properties of HDPE/EPDM blends. Arab J Chem 4:71–77

Publisher's Note Springer Nature remains neutral with regard to jurisdictional claims in published maps and institutional affiliations.